

Ab Initio Theory of the Impact from Grain Boundaries and Substitutional Defects on Superconducting Nb₃Sn

Michelle M. Kelley, Nathan S. Sitaraman, and Tomás A. Arias
Department of Physics, Cornell University, Ithaca, New York 14853, USA
(Dated: May 26, 2020)

Grain boundaries play a critical role in applications of superconducting Nb₃Sn: in dc applications, grain boundaries preserve the material's intrinsically high critical-current by pinning flux, while in ac applications grain boundaries can provide weak points for flux entry and lead to significant dissipation. We present the first *ab initio* study to investigate the physics of different boundary types in Nb₃Sn using density functional theory. We identify an energetically favorable selection of tilt and twist grain boundaries of distinct orientations. We find that clean grain boundaries free of point defects reduce the Fermi-level density of states by a factor of two, an effect that decays back to the bulk electronic structure $\sim 1\text{--}1.5$ nm from the boundary. We further calculate the binding free-energies of tin substitutional defects to multiple boundaries, finding a strong electronic interaction that extends to a distance comparable to that of the reduction of density of states. Associated with this interaction, we discover a universal trend in defect electronic entropies near a boundary. We probe the effects of defect segregation on grain boundary electronic structure and calculate the impact of substitutional impurities on the Fermi-level density of states in the vicinity of a grain boundary, finding that titanium and tantalum have little impact regardless of placement, whereas tin, copper, and niobium defects each have a significant impact but only on sites away from the boundary core. Finally, we consider how all of these effects impact the local superconducting transition temperature T_c as a function of distance from the boundary plane.

I. INTRODUCTION

Nb₃Sn is a type-II superconductor and belongs to the A15 class of superconductors which held the record for highest T_c from 1954–1968 [1, 2]. With a critical temperature of 18 K and the ability to operate in high fields, Nb₃Sn is widely used in applications for high-field magnets in particle accelerators, fusion reactors, nuclear magnetic resonance, magnetic resonance imaging and non-magnet applications such as superconducting radio frequency (SRF) cavities [3–8].

Superconducting Nb₃Sn lives in an interesting regime sharing features of both elemental and high- T_c superconductors. Grain boundaries are known to degrade the superconducting properties of the cuprates and other modern high- T_c superconductors, providing structural disorder on length scales comparable to their notably short coherence lengths [9–12]. Nb₃Sn is a conventional superconductor based on the elemental superconductor niobium, but unlike niobium which has a coherence length of ~ 50 nm, Nb₃Sn has a coherence length of ~ 3 nm, approaching the scale of structural disorder from grain boundaries [13–15]. There is even speculation that grain boundaries in Nb₃Sn may exhibit Josephson-like effects [16–18].

Optimizing the influence of grain boundaries in Nb₃Sn depends on the application. In dc applications such as superconducting wires, high-density grain boundaries provide needed pinning centers to prevent vortices from limiting the critical-current density [4, 19, 20]. In ac applications such as SRF cavities, significant dissipation arises once flux penetrates the material and grain boundaries can provide unwanted nucleation sites [15, 21–23].

Disorder and stoichiometric variations within Nb₃Sn

are known to have a profound influence on the material's properties [13, 24–26], and tin segregation at grain boundaries has been observed experimentally [20, 27, 28]. Strong gradients of tin composition at grain boundaries can reduce the critical current density, the flux pinning force and flux pinning scaling field in superconducting wires [29–31]. Additionally, highly degraded quality factors have been observed in SRF cavities with prominent tin segregation at grain boundaries [28].

Nb₃Sn is often engineered with ternary elements for various optimizations. Additions of copper help Nb₃Sn growth by lowering the A15 formation temperature, and additions of titanium and tantalum, prevent the transformation into the tetragonal phase [13, 25, 27]. Segregation of these impurities at and around grain boundaries have been observed [20]. While the flux pinning force is known to scale with grain boundary density, it can also be affected by other defects at the boundary [32, 33]. As Nb₃Sn continues to be optimized, distinguishing the effects among defects opens up exciting prospects for grain boundary engineering [34].

We study the influence of grain boundaries on the properties of Nb₃Sn from first principles using density functional theory. We identify a selection of energetically favorable structures featuring both tilt and twist grain boundaries, study the impact of boundaries on the electronic structure, and the behavior of defects near a boundary. Motivated by recent experiments that found highly degraded quality factors in Nb₃Sn SRF cavities with excess tin at grain boundaries, we calculate how the local superconducting properties are affected by a boundary containing their measured tin concentration profile [28].

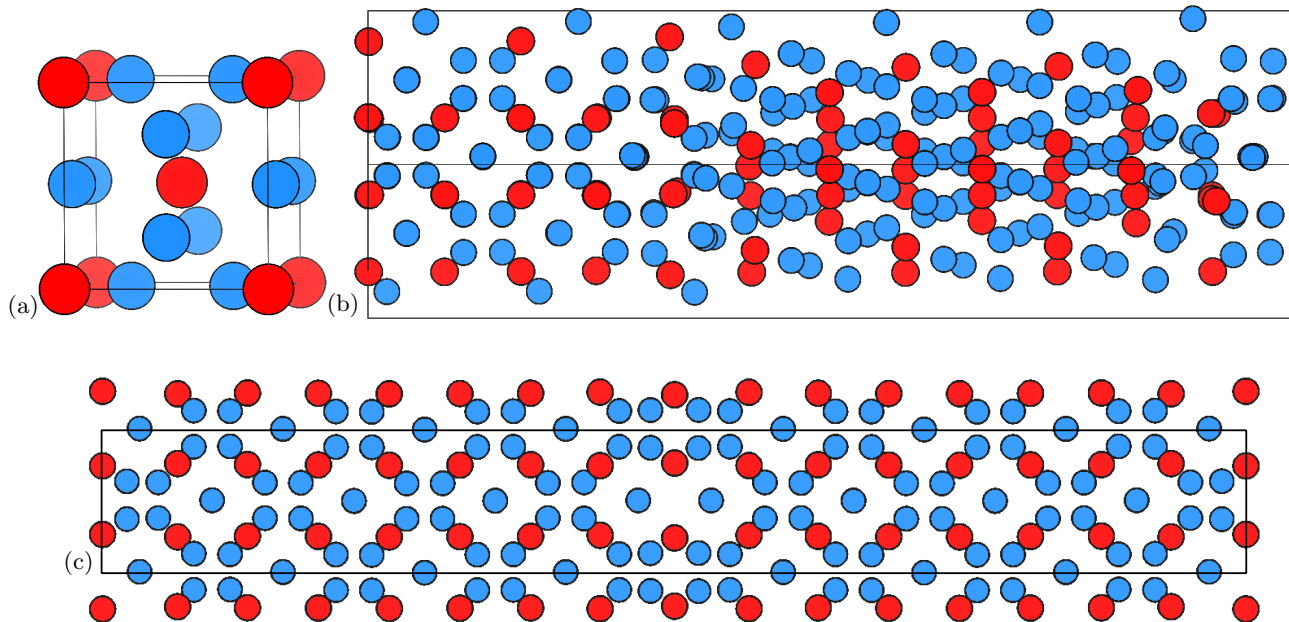


FIG. 1. Atomic structures with niobium colored in blue and tin in red. (a) The unit cell of cubic A15 Nb_3Sn with the tin atoms forming a bcc-lattice and chains of niobium atoms running along the faces of the cubes in the three orthogonal directions. Relaxed atomic positions in (b) the (110)-twist boundary cell and (c) the (110)-tilt boundary cell reported in Table I.

II. METHODS

We perform density functional theory calculations within the pseudopotential framework using open-source plane wave software JDFTx [35]. The electronic states are calculated for the outer electrons of niobium ($4p^6 5s^2 4d^3$) and tin ($4d^{10} 5s^2 5p^2$) while the atomic cores are treated using ultrasoft pseudopotentials [36]. We use the Perdew-Burke-Ernzerhof (PBE) approximation to the exchange-correlation functional and employ a 12 Hartree planewave cutoff energy [37]. Defect energies are calculated at high electronic temperatures using a Fermi function with a 5 milliHartree electronic temperature, chosen to be close to the experimental growth temperature of Nb_3Sn cavities [15, 38, 39]. Parameters relevant to our superconductivity analysis such as the densities of states are calculated at zero-temperature using the cold-smearing method developed by Marzari where we again use a smearing width of 5 mH to maintain the same tolerance with respect to k-point sampling [40]. With these parameters, we calculate the lattice parameter for cubic A15 Nb_3Sn to be 5.271 Å, in excellent agreement to its measured value of 5.289 Å [13, 41]. For cubic A15 Nb_3Sn we sample 6^3 k-points in the Brillouin zone then transform to a maximally localized Wannier function basis to perform a dense Monte Carlo sampling to accurately calculate the density of states [42]. The k-point meshes for the grain-boundary cells are chosen to have a sampling density comparable to the unit cell calculation, and their density of states are calculated with a tetrahedral interpolation scheme. All results of the boundary cells involve

fully relaxed internal atomic coordinates. We also consider the effects of lattice relaxation by setting the interfacial plane at the bulk lattice constant and allow the lattice to relax along the boundary plane normal. We note, however, that the lattice relaxations do not significantly change any of the boundary energies so the results reported below are calculated at the bulk lattice constant.

III. BOUNDARY STRUCTURES AND ENERGIES

Nb_3Sn is an intermetallic alloy in the A15 phase; its cubic unit cell is displayed in Fig. 1(a) [43]. The A15 structure is characterized with one species of atom (tin) forming a bcc-lattice and each cube face containing two of the other atomic species (niobium). The two atoms on each cube face form one-dimensional chains of transition metals in the three orthogonal directions [44]. This particular structure is characteristically accompanied with a high Fermi level density of states [41].

The electronic structure and the superconducting properties of A15 materials are known to be sensitive to point defects, particularly when the structure strays away from its ideal stoichiometry [24, 26]. Here, we report the impact of grain boundaries on various properties of Nb_3Sn and how these extended defects may interact with point defects. To our knowledge, the only existing first-principles studies on grain boundaries in this material are an unpublished thesis [45] and a recent study that looked at three defect sites in one boundary cell but

TABLE I. List of boundaries labeled with their interfacial plane and boundary type, their misorientation angle, the distance between boundaries, and their relaxed grain boundary energies, γ .

Boundary	θ	Grain Separation	γ (mJ m ⁻²)
(110)-tilt	90°	2.99 nm	1455
(112)-tilt	70.5°	2.59 nm	840
(120)-tilt	53.1°	2.36 nm	1440
(100)-twist	90°	2.64 nm	650
(110)-twist	70.5°	2.36 nm	1300

included no results on the electronic structure [28].

A grain boundary refers to the interface between two crystal grains of differing orientations and can be described by their grain boundary plane and misorientation angle [46]. The two idealized boundary types are the twist and tilt boundary, and an example of each is shown in Fig. 1(b) and (c) respectively.

Grain boundaries are planar defects with excess free energy per unit area. For a simple estimate of a grain boundary energy, we follow Ref. 47 to estimate the amount of elastic work done to create a surface based on the material's elastic modulus. Since Nb₃Sn has a elastic modulus of ~ 127 GPa [48], we expect grain boundary energies roughly in the range of 700–1500 mJ m⁻².

Table I lists a selection of relaxed tilt and twist grain boundary cells. Their grain boundary energies are calculated using

$$\gamma = \frac{(E_{GB} - E_{bulk})}{2A}, \quad (1)$$

where E_{GB} and E_{bulk} refer to the total energies of the boundary structure and the bulk structure of the same size, and A is the interfacial area of the boundary. All table entries involve structures with exactly a 3:1 stoichiometry except for the (100)-twist, where we remove two Nb atoms and place them in bulk Nb because Nb₃Sn is often grown on a Nb substrate.

IV. THE IMPACT OF A CLEAN BOUNDARY ON ELECTRONIC STRUCTURE

A notable feature of the A15 superconductors is their high Fermi-level density of states. For weakly-coupled superconductors, the critical temperature can be described with the BCS equation, which exhibits an exponential dependence on the Fermi-level density of states $N(0)$.

$$k_B T_c = 1.14 E_D e^{-1/N(0)V} \quad (2)$$

Strongly-coupled superconductors such as Nb₃Sn are more accurately described with Eliashberg theory applied within a density-functional framework to calculate the electron-phonon coupling, V [49–51]. The critical temperature in this case is determined with the phenomeno-

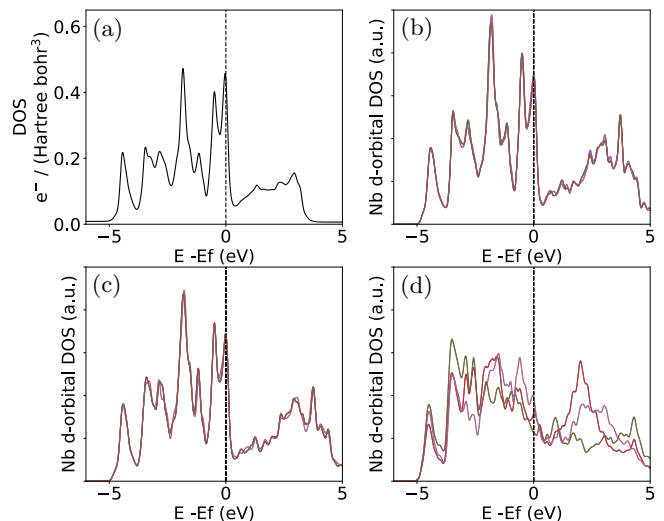


FIG. 2. (a) Total density of states in bulk Nb₃Sn calculated in a maximally localized Wannier function basis. The d-orbital projected density of states on niobium atoms plotted on the same scale in (b) a pure bulk cell, and in the (c) bulk region and (d) grain boundary core of (112)-tilt boundary cell. Each of (b–d) are plotted on the same scale for direct comparison.

logical McMillan formula, which exhibits the same exponential dependence on $N(0)$ as Eq. 2 [52].

We calculate the total density of states of cubic A15 Nb₃Sn in a maximally-localized Wannier function basis in order to resolve sharp features in k-space. The total density of states is shown in Fig. 2(a). To visualize the contribution of the 1D niobium chains, we plot the partial projected density of states along d-orbitals of bulk niobium atoms in Fig. 2(b).

The high peak in the density of states at the Fermi-level varies rapidly on small energy scales, dropping by more than a factor of 2 within 0.2 eV. This feature is a result of the conducting d-orbitals of the long 1D-chains of niobium atoms, or other transition metals for the other A15 superconductors [13, 41]. This is confirmed by comparing Fig. 2(a) and (b), showing the direct correspondence between the niobium atom d-orbital projected density of states with the total density of states. Once these chains are disturbed by defects, the high Fermi-level density of states is lost [26].

We now investigate how an extended defect such as a grain boundary impacts the density of states. In Fig. 2 we plot the d-orbital projected density of states of (c) six niobium atoms in the bulk region and (d) six niobium atoms on the grain boundary core in the (112)-tilt boundary. We note that Fig. 2(b–d) are plotted on the same scale and can be compared relative to one another. The niobium atoms in the bulk region of the boundary cell have density of states nearly indistinguishable from that of niobium atoms in infinite bulk Nb₃Sn, showing that our cell is converged with respect to the boundary separation. For the niobium atoms on the grain-boundary

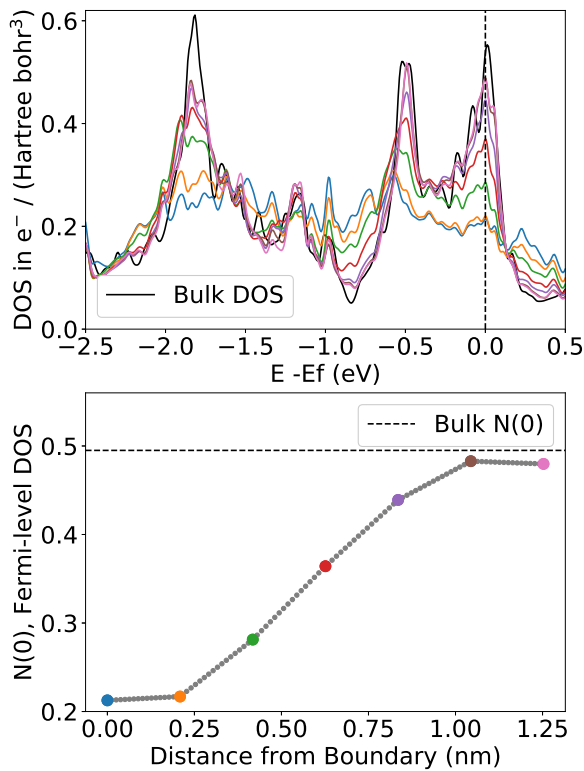


FIG. 3. Local density of states curves across slabs in the (112)-tilt boundary cell (top). The corresponding Fermi-level density of states profile as a function of distance from the boundary (bottom).

core, the Fermi-level density of states is significantly reduced, roughly by a factor of two.

To see how far this reduction extends into the crystal, we perform local density of states calculations, averaging over slabs perpendicular to the boundary plane. Results from this local density of states analysis and the corresponding profile of the Fermi-level density of states are plotted in Fig. 3. We find that the factor of two reduction in the Fermi-level density of states at the grain boundary core decays smoothly back to the bulk value, in ~ 1 nm from this boundary, and in ~ 1 – 1.5 nm from boundaries in general.

V. INTERACTIONS BETWEEN BOUNDARIES AND POINT DEFECTS

A. Binding energy of tin antisite defects to a boundary

Understanding how defects interact with grain boundaries in Nb_3Sn can help advance applications of the material. The diffusivity of tin atoms through grain boundaries relative to bulk is important for Nb_3Sn growth [33]. Tin defects at grain boundaries have been observed to be particularly detrimental to the material in multiple

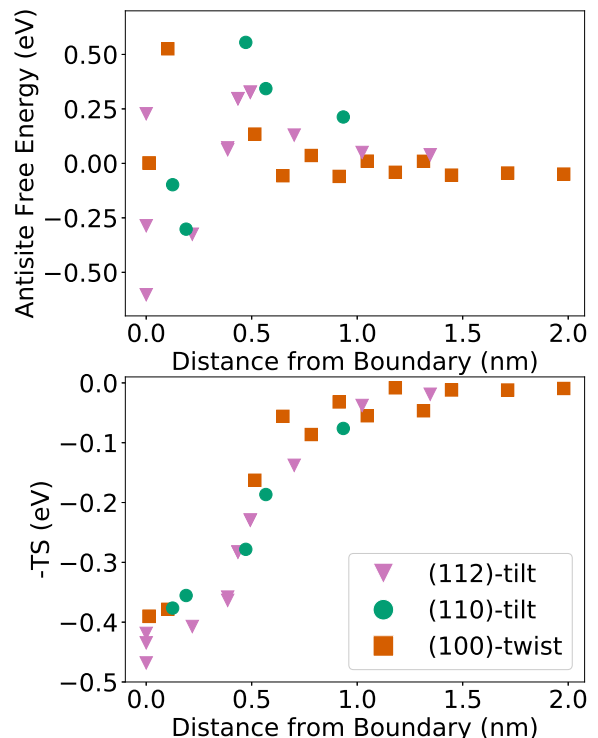


FIG. 4. Binding free-energy of Sn_{Nb} defects to a boundary (top) and the corresponding electronic entropy contribution to the free energy (bottom).

applications [4, 20, 28]. Accordingly, we first turn our attention towards tin defects near a grain boundary.

The prevailing tin defect in $\text{A15 Nb}_3\text{Sn}$ consists of a tin atom sitting on niobium site, denoted as Sn_{Nb} [53]. In the top panel of Fig. 4, we plot the defect free-energies of tin substitutions relative to a tin substitution in bulk as a function of distance from a boundary in our (110)-tilt, (112)-tilt, and (100)-twist boundary cells. The bottom panel of Fig. 4 displays the electronic entropy component of these free energies.

We find a strong, extended electronic interaction between tin antisite defects and grain boundaries that decays to bulk behavior within ~ 1 – 1.5 nm. Near the boundary, we find a range of attractive and repulsive sites in all three boundary cells and conclude that the trends in these antisite free-energies may be complicated by structural details of the boundaries. Remarkably, however, the electronic entropy components of these free energies collapse onto a single curve when plotted as a function of distance and explain the magnitude and range of the interaction with the boundary. There are significant free-energy gains approaching ~ 0.5 eV favoring segregation of tin defects towards grain boundaries.

B. Impact of substitutional defects on a boundary's electronic structure

To gain insight on the combined effect of defects and grain boundaries on superconductivity in this material, we look to see how various defects impact the local Fermi-level density of states. In light of the nearly universal electronic interactions observed above, we consider for these investigations a single example for a case study, selecting the (112)-tilt boundary for its relatively low energy and non-trivial structure.

Because of the prevalence of metallic substitutions detected at grain boundaries in Nb_3Sn [20, 27, 28], we consider the two antisite defects Sn_{Nb} and Nb_{Sn} as well as defects of common ternary additions Ti_{Nb} , Ta_{Nb} , and Cu_{Sn} [32, 54]. For a defect on the grain boundary core, we put the defect atom on the lowest-energy defect site identified within the core of the (112)-tilt boundary. We compare the effect of this substitutional defect to the same defect in bulk by placing the same defect in the bulk region in a second calculation. Fig. 5(b) indicates the specific locations of niobium and tin sites for both bulk and grain boundary defects.

Earlier we found the effect of a clean grain boundary on the local Fermi-level density of states. Here, we repeat the same procedure in the presence of one substitutional defect. Fig. 5(a) compares the profiles of the Fermi-level density of states resulting from Sn_{Nb} , Nb_{Sn} , Ti_{Nb} , Ta_{Nb} , and Cu_{Sn} defects. The profile of the clean grain boundary free of point defects is displayed in Fig. 3(b).

We find that, because a clean grain boundary itself already degrades the Fermi-level density of states by a factor of two, placing a point defect on the grain boundary core does not further degrade the density of states. In contrast, placing defects in the bulk region allows for greater impact on the local Fermi-level density of states. The most notable degradation arises from the Sn_{Nb} , Nb_{Sn} , and Cu_{Sn} defects in bulk. These particular point defects profoundly disturb the conducting d-orbitals along the niobium chains. Interestingly, the Ti_{Nb} and Ta_{Nb} defects in bulk preserve most of the Fermi-level density of states, likely due to the chemical similarity of these elements to niobium. This disparity between defects underscores the importance of distinguishing variations in stoichiometry arising from ternary elements from intrinsic variations in tin content which can have entirely different consequences.

VI. SUPERCONDUCTIVITY AND GRAIN BOUNDARY COMPOSITION

Lastly, we consider the effects of grain boundary composition on the local superconducting properties. We calculate the impact of a grain boundary with tin-concentrations corresponding to measurements of Ref. 28 that reported a Gibbsian interfacial excess of 10–20 tin atoms/ nm^2 . We model their observations in our (110)-

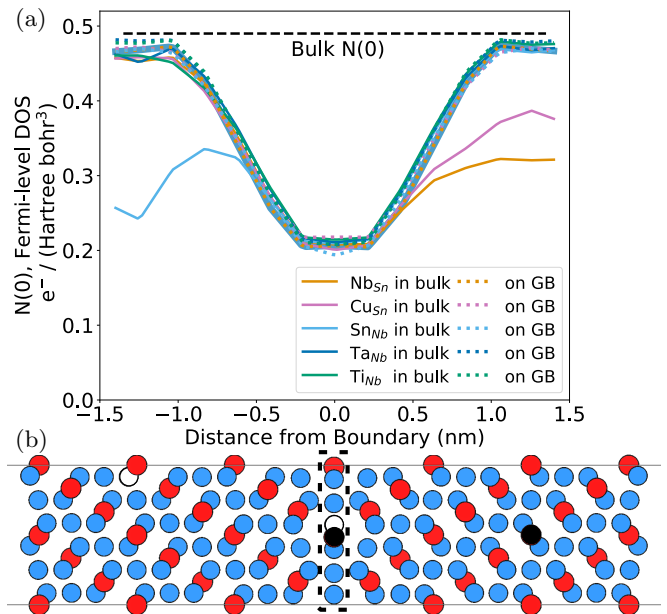


FIG. 5. (a) Local Fermi-level density of states across the (112)-tilt boundary including one defect atom on the grain boundary core (dotted lines) or in bulk (solid lines). (b) Atomic configuration displaying the tin and niobium atoms (red, blue), and the tin and niobium sites for substitutional defects (black, white).

tilt boundary cell containing the concentration profile displayed in Fig. 6(b), where the atomic positions are averaged over a Gaussian corresponding to the lateral resolution of their probe. Ref. 28 reports a ~ 3 nm wide boundary with a maximum tin concentration at 35%, and the gray curve in Fig. 6(b) approximates this with a Gaussian displaying a peak concentration of 35% and a width of $4\sigma = 3$ nm. To ensure we do not overestimate the effects of tin-segregated grain boundaries, we add a modest excess of 10 tin atoms/ nm^2 , spanning a slightly smaller width than that reported. Finally, the local Fermi-level density of states profiles from the clean (110)-tilt and the same structure with excess tin atoms are displayed in Fig. 6(c).

The depression in the Fermi-level density of states from the tin-rich grain is only slightly deeper but extends much further than that of its stoichiometric counterpart. To understand the impact of the clean and tin-rich boundary structures on the local superconducting transition temperature T_c , we note that first principle studies in Nb_3Sn have established that the primary impact on T_c in this material comes from the Fermi-level density of states as opposed to other factors. Specifically, a first principles study on the impact on strain in Nb_3Sn showed that $\sim 80\%$ of the degradation of the superconducting properties from strain comes from the reduction in the Fermi-level density of states [55], and another first principles study on antisite defects in Nb_3Sn also found T_c

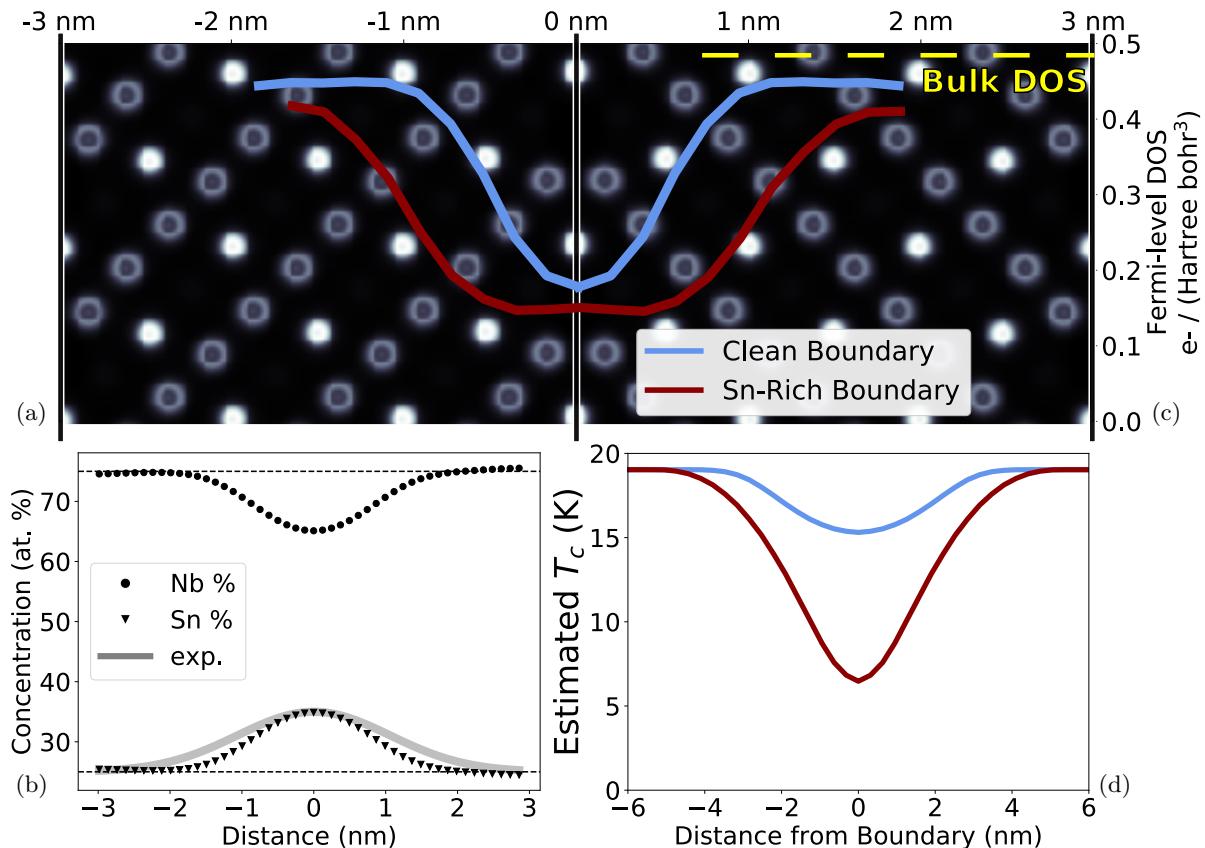


FIG. 6. (a) Two-dimensional slice of the electron density in the (110)-tilt boundary. (b) Atomic concentration profile added to the (110)-tilt boundary to simulate the interfacial excess measurements reported in Ref. 28, approximated by the gray curve. (c) Local Fermi-level density of states profiles around the clean and tin-rich (110)-tilt boundaries. (d) Resulting estimates of a local superconducting transition temperature T_c from averaging the profiles over the volume of a Cooper pair.

to be strongly correlated with the Fermi-level density of states [26]. To provide local values for T_c , the Fermi-level density of states must be averaged over the appropriate length scale of a Cooper pair, specifically the coherence length. Fig. 6(d) shows our resulting estimates for the local transition temperature, obtained by integrating the density of states profiles in Fig. 6(c) over a sphere of radius 3 nm to coincide with the coherence length of Nb_3Sn .

We find the reduction in T_c to be wider and much deeper for the tin-rich boundary than for the clean boundary as a result of the much wider depression in the local Fermi-level density of states. The local T_c around a clean grain boundary is barely degraded because the depression in the density of states has a diameter of ~ 2 nm while a Cooper pair has a radius of 3 nm. However, a boundary filled with tin-defects widens the depression in the density of states, to the detriment of the local super-

conducting properties. This result correlates well with the findings of Ref. 28, reporting degraded quality factors from Nb_3Sn SRF cavities containing tin-rich grain boundaries and high quality factors from cavities containing clean grain boundaries. We also expect degradations in the local superconducting properties from boundaries filled with Nb_{Sn} and Cu_{Sn} defects, and note that similar effects on copper's influence have been observed [56].

Grain boundaries with low T_c are a candidate mechanism that lowers the first vortex entry field in Nb_3Sn SRF cavities, and enhancing flux pinning in Nb_3Sn superconducting wires is the only opportunity to improve critical current densities [4, 57]. Ginzburg-Landau simulations can build off of these local T_c estimates to further our understanding of flux penetration and pinning at grain boundaries in Nb_3Sn [21, 23, 30].

VII. CONCLUSIONS

This paper presents the first *ab initio* investigation of the physics of different boundary types in Nb₃Sn. To our knowledge, this study is the first to investigate twist boundaries in addition to tilts and to include boundary planes with distinct orientations. We present a selection of energetically favorable structures and identify structures at the low end of the expected energy range for both boundary types. These representative structures provide a foundation to examine the physics of grain boundaries in Nb₃Sn broadly.

We present the impact a grain boundary has on the electronic structure and find that the Fermi-level density of states is significantly degraded, which is expected from the disrupted niobium chains in the A15 phase. We find that grain boundaries have a striking long-range effect on the electronic structure, where the depression in the density of states extends out to ~ 1 – 1.5 nm.

Looking towards the impact of a boundary's electronic structure on the binding energy of defects, we find a strong electronic interaction that also extends out ~ 1 – 1.5 nm. Defect free-energies near the boundary are complicated by local structural details, but the electronic entropy contributions to the defect-boundary interaction remarkably collapse onto a single curve and provide a ready explanation of the magnitude and range of the interaction. Finally, we predict grain boundaries to have a full-width interaction range of ~ 2 – 3 nm with point defects, correlating well with the atomic content measurements [20, 27, 28].

Defects also affect the electronic structure of grain boundaries. We find that point defects on the grain boundary core at low concentrations do not degrade the density of states much beyond the impact of the boundary itself. We do find that point defects away from the boundary have more of a relative impact, with bulk Sn_{Nb}, Nb_{Sn}, Cu_{Sn} defects in particular being severely detrimen-

tal. We also find evidence that other defects such as Ti_{Nb} and Ta_{Nb} can be used as dopants without severely impacting the electronic structure of the material.

Finally, we introduce a model for a local superconducting transition temperature T_c in the vicinity of a grain boundary. Given the damaging impact of Sn_{Nb} defects on the Fermi-level density of states and the fact that the transition temperature in Nb₃Sn is most sensitive to the density of states, we calculate the effect of a boundary containing a tin concentration profile analogous to those observed in experiment. We find a wide depression on the Fermi-level density of states in the tin-rich boundary that extends further than from a clean boundary of the same structure. This wide depression causes a large reduction in T_c around the tin-rich boundary while the local T_c around a clean boundary is barely degraded. From this, we conclude that grain boundaries with excess tin are indeed more detrimental to superconductivity than are clean grain boundaries, and affirm that controlling tin defects is crucial for applications of superconducting Nb₃Sn.

VIII. ACKNOWLEDGEMENTS

We would like to thank Jim Sethna, David Muller, Matthias Liepe, and Ryan Porter of Cornell University and Sam Posen of Fermilab for insightful discussions regarding grain boundaries and Nb₃Sn, Jaeyel Lee and David Seidman of Northwestern University for sharing their experimental measurements, and Ravishankar Sundararaman of Rensselaer Polytechnic Institute for all the momentous first-principles software he continues to develop.

This work was supported by the US National Science Foundation under award PHY-1549132, the Center for Bright Beams.

-
- [1] D. Dew-Hughes, *Cryogenics* **15**, 435 (1975).
 - [2] G. R. Stewart, *Physica C: Superconductivity and its Applications* **514**, 28 (2015), arXiv:1505.06393.
 - [3] A. Echarri and M. Spadoni, *Cryogenics* **11**, 274 (1971).
 - [4] X. Xu, *Superconductor Science and Technology* **30**, 10.1088/1361-6668/aa7976 (2017).
 - [5] J. A. Parrell, M. B. Field, Y. Zhang, and S. Hong, *IEEE Transactions on Applied Superconductivity* **15**, 1200 (2005).
 - [6] R. G. Sharma, *Superconductivity: Basics and Applications to Magnets*, Springer Series in Materials Science (Springer International Publishing, 2015).
 - [7] T. Baig, Z. Yao, D. Doll, M. Tomsic, and M. Martens, *Superconductor Science and Technology* **27**, 10.1088/0953-2048/27/12/125012 (2014).
 - [8] S. Posen, M. Liepe, and D. L. Hall, *Applied Physics Letters* **106**, 0 (2015).
 - [9] H. Hilgenkamp and J. Mannhart, *Reviews of Modern Physics* **74**, 485 (2002).
 - [10] S. E. Babcock and J. L. Vargas, *Annual Review of Materials Science* **25**, 193 (1995).
 - [11] A. Gurevich, *Nature Materials* **10**, 255 (2011).
 - [12] T. Katase, Y. Ishimaru, A. Tsukamoto, H. Hiramatsu, T. Kamiya, K. Tanabe, and H. Hosono, *Nature Communications* **2**, 10.1038/ncomms1419 (2011).
 - [13] A. Godeke, *Superconductor Science and Technology* **19**, 10.1088/0953-2048/19/8/R02 (2006), arXiv:0606303 [cond-mat].
 - [14] J. Draskovic, T. R. Lemberger, B. Peters, F. Yang, J. Ku, A. Bezryadin, and S. Wang, *Physical Review B - Condensed Matter and Materials Physics* **88**, 1 (2013), arXiv:1403.6856.
 - [15] S. Posen and D. L. Hall, *Superconductor Science and Technology* **30**, 10.1088/1361-6668/30/3/033004 (2017).
 - [16] A. Gurevich, *Phys. Rev. B* **46**, 5 (1992).
 - [17] D. L. Hall, M. Liepe, R. D. Porter, P. Cueva, D. B. Liarte,

- D. A. Muller, and J. P. Sethna, 18th International Conference on RF Superconductivity , 840 (2017).
- [18] A. Sheikhzada and A. Gurevich, *Physica C: Superconductivity and its Applications* **506**, 59 (2014).
- [19] R. M. Scanlan, W. A. Fietz, and E. F. Koch, *Journal of Applied Physics* **46**, 2244 (1975).
- [20] M. J. Sandim, D. Tytko, A. Kostka, P. Choi, S. Awaji, K. Watanabe, and D. Raabe, *Superconductor Science and Technology* **26**, 10.1088/0953-2048/26/5/055008 (2013).
- [21] M. K. Transtrum, G. Catelani, and J. P. Sethna, *Physical Review B - Condensed Matter and Materials Physics* **83**, 1 (2011).
- [22] D. B. Liarte, S. Posen, M. K. Transtrum, G. Catelani, M. Liepe, and J. P. Sethna, *Superconductor Science and Technology* **30**, 0 (2017).
- [23] J. Carlson, A. Pack, M. K. Transtrum, J. Lee, D. N. Seidman, D. B. Liarte, N. Sitaraman, A. Senanian, J. P. Sethna, T. Arias, and S. Posen, (2020), arXiv:2003.03362.
- [24] M. G. T. M. ten Kate, M. M. J. Dhalle, D. R. Dietderich, A. Godeke, F. Hellman, H. H. J. M. G. T. Mentink, M. M. J. Dhalle, D. R. Dietderich, A. Godeke, F. Hellman, and H. H. J. ten Kate, *Superconductor Science and Technology* **30**, 25006 (2017).
- [25] R. Flükiger, D. Uglietti, C. Senatore, and F. Buta, *Cryogenics* **48**, 293 (2008).
- [26] N. S. Sitaraman, J. Carlson, A. R. Pack, R. D. Porter, M. U. Liepe, M. K. Transtrum, and T. A. Arias, (2019), arXiv:1912.07576.
- [27] M. Suenaga and W. Jansen, *Applied Physics Letters* **43**, 791 (1983).
- [28] J. Lee, Z. Mao, K. He, Z. H. Sung, T. Spina, S. I. Baik, D. L. Hall, M. Liepe, D. N. Seidman, and S. Posen, *Acta Materialia* **188**, 155 (2020).
- [29] L. D. Cooley, C. M. Fischer, P. J. Lee, and D. C. Larbalestier, *Journal of Applied Physics* **96**, 2122 (2004).
- [30] Y. Li and Y. Gao, *Scientific Reports* **7**, 1 (2017).
- [31] T. Baumgartner, S. Pfeiffer, J. Bernardi, A. Ballarino, and M. Eisterer, *Superconductor Science and Technology* **31**, 10.1088/1361-6668/aac87e (2018).
- [32] J. D. Livingston, *Physica Status Solidi (a)* **44**, 295 (1977).
- [33] K. Osamura, S. Ochiai, S. Kondo, M. Namatame, and M. Nosaki, *Journal of Materials Science* **21**, 1509 (1986).
- [34] D. Raabe, M. Herbig, S. Sandlöbes, Y. Li, D. Tytko, M. Kuzmina, D. Ponge, and P. P. Choi, *Current Opinion in Solid State and Materials Science* **18**, 253 (2014).
- [35] R. Sundararaman, K. Letchworth-Weaver, K. A. Schwarz, D. Gunceler, Y. Ozhabes, and T. A. Arias, *SoftwareX* **6**, 278 (2017), arXiv:1708.03621.
- [36] K. F. Garrity, J. W. Bennett, K. M. Rabe, and D. Vanderbilt, *Computational Materials Science* **81**, 446 (2014), arXiv:1305.5973.
- [37] J. P. Perdew, K. Burke, and M. Ernzerhof, *Physical Review Letters* **77**, 3865 (1996).
- [38] J. Lee, S. Posen, Z. Mao, Y. Trenikhina, K. He, D. L. Hall, M. Liepe, and D. N. Seidman, *Superconductor Science and Technology* **32**, 10.1088/1361-6668/aaf268 (2019), arXiv:1807.03898.
- [39] R. D. Porter, T. Arias, P. Cueva, D. L. Hall, M. Liepe, J. T. Maniscalco, D. A. Muller, and N. Sitaraman, *Proceedings of LINAC2018* , 462 (2018).
- [40] N. Marzari, D. Vanderbilt, A. De Vita, and M. C. Payne, *Physical Review Letters* **82**, 3296 (1999), arXiv:9903147 [cond-mat].
- [41] H. Devantay, J. L. Jorda, M. Decroux, J. Muller, and R. Flükiger, *Journal of Materials Science* **16**, 2145 (1981).
- [42] N. Marzari and D. Vanderbilt, *Physical Review B - Condensed Matter and Materials Physics* **56**, 12847 (1997), arXiv:9707145 [cond-mat].
- [43] K. Momma and F. Izumi, *Journal of Applied Crystallography* **44**, 1272 (2011).
- [44] R. B. King, *Inorganic Chemistry* **29**, 2164 (1990).
- [45] P. J. P. BYRNE, *Superconducting Properties from First Principles Calculations : An Ab-Initio Study of the properties of Superconductors under Perturbations*, Ph.D. thesis, Durham University (2017).
- [46] R. E. Smallman and A. H. W. Ngan, in *Modern Physical Metallurgy (Eighth Edition)*, edited by R. E. Smallman and A. H. W. Ngan (Butterworth-Heinemann, Oxford, 2014) eighth edi ed., pp. 415–442.
- [47] G. S. Rohrer, *Journal of Materials Science* **46**, 5881 (2011).
- [48] M. Hojo, T. Matsuoka, M. Hashimoto, M. Tanaka, M. Sugano, S. Ochiai, and K. Miyashita, *Physica C: Superconductivity and its Applications* **445-448**, 814 (2006).
- [49] G. M. Eliashberg, *Sov. Phys. - JETP (Engl. Transl.); (United States)* (1960).
- [50] A. M. Brown, R. Sundararaman, P. Narang, W. A. Goddard, and H. A. Atwater, *Physical Review B* **94**, 1 (2016), arXiv:1602.00625.
- [51] A. M. Brown, R. Sundararaman, P. Narang, W. A. Goddard, and H. A. Atwater, *ACS Nano* **10**, 957 (2016).
- [52] W. L. McMillan, *PhysGical Review* **167**, 331 (1968).
- [53] R. Besson, S. Guyot, and A. Legris, *Physical Review B - Condensed Matter and Materials Physics* **75**, 1 (2007).
- [54] J. Taftø, M. Suenaga, and D. O. Welch, *Journal of Applied Physics* **55**, 4330 (1984).
- [55] A. Godeke, F. Hellman, H. H. Kate, and M. G. Mentink, *Superconductor Science and Technology* **31**, 10.1088/1361-6668/aad980 (2018).
- [56] C. A. Rodrigues and D. Rodrigues, *IEEE Transactions on Applied Superconductivity* **17**, 2627 (2007).
- [57] A. R. Pack, J. Carlson, S. Wadsworth, and M. K. Transtrum, (2019), arXiv:1911.02132.